crystals

MDPI

Article

Site-Preference, Electronic, Magnetic, and Half-Metal Properties of Full-Heusler Sc_2VGe and a Discussion on the Uniform Strain and Tetragonal Deformation Effects

Zongbin Chen [1], Heju Xu [1], Yongchun Gao [1,*], Xiaotian Wang [2,*] and Tie Yang [2,*]

[1] Department of Physics, College of Science, North China University of Science and Technology, Tangshan 063210, China
[2] School of Physical Science and Technology, Southwest University, Chongqing 400715, China
* Correspondence: gaoyc1963@ncst.edu.cn (Y.G.); xiaotianwang@swu.edu.cn (X.W.); yangtie@swu.edu.cn (T.Y.)

Received: 12 August 2019; Accepted: 20 August 2019; Published: 27 August 2019

Abstract: A hypothetical full-Heusler alloy, Sc_2VGe, was analyzed, and the comparison between the XA and $L2_1$ structures of this alloy was studied based on first-principles calculations. We found that the $L2_1$-type structure was more stable than the XA one. Further, the electronic structures of both types of structure were also investigated based on the calculated band structures. Results show that the physical nature of $L2_1$-type Sc_2VGe is metallic; however, XA-type Sc_2VGe is a half-metal (HM) with 100% spin polarization. When XA-type Sc_2VGe is at its equilibrium lattice parameter, its total magnetic moment is 3 μ_B, and its total magnetism is mainly attributed to the V atom. The effects of uniform strain and tetragonal lattice distortion on the electronic structures and half-metallic states of XA-type Sc_2VGe were also studied. All the aforementioned results indicate that XA-type Sc_2VGe would be an ideal candidate for spintronics studies, such as spin generation and injection.

Keywords: full-heusler; half-metal; direct band gap; first principles

1. Introduction

Since 1983 Groot et al. [1] reported NiMnSb was a half-metal (HM) for the first time, Heusler alloys, including half-Heulser (HH) [2–5] and full-Heusler (FH) alloys [6–15], have attracted extensive attention from researchers. HMs [16–20] have broad application prospects in the field of spintronics or magnetoelectronics due to the theoretical prediction of their 100% spin polarization.

In recent years, HH compounds with HM properties have been widely reported [21–23]. Some examplesare as follows: in 2011, Chen et al. [24] found that GeKCa and SnKCa exhibit HM properties, and that these alloys have large HM band gap values of 0.28 eV and 0.27 eV, respectively. In 2012, Yao et al. [25] found that CoCrP and CoCrAs have HM properties with HM band gap values of 0.46 eV and 0.50 eV, respectively. It was also found that, in terms of lattice distortion, the HM properties of these alloys can be maintained in the range of −4.8% to 6.6% and −7.7% to 4.5%, respectively. The discovery of the presence of HM properties in HH alloys has led to the availability of more options for spintronics materials [26,27].

A series of FH compounds with HM properties were also reported by researchers [28]. For example, Kogachi et al. [29] studied the electronic and magnetic properties of Co_2MnZ (Z = Si, Ge, Sn). Liu et al. [30] investigated the electronic structures of Mn_2CoZ (Z = Al, Si, Ge, Sn, Sb) in detail and found two mechanisms to induce the band gap for minority spin states near the Fermi level; Wang et al. [31] studied the electronic and magnetic properties of FH alloy Zr_2CoZ (Z = Al, Ga, In, Si, Ge, Sn, Pb, Sb) and found that the half-metallicities are robust against lattice distortion; Wang et al. also studied the site preferences of the Titanium-based [32] and Hf_2V-based [33] FH alloys, and found that most of these alloys are likely to form the $L2_1$ structure instead of the XA structure. Thus, the traditional site-preference rule (SPR) may not be suitable for all FH alloys, such as X_2YZ, where X is a low-valent transition metal element, such as, Ti, Zr, Sc, and Hf.

There are also some reports about the scandium-based (SB) FH alloys. In 2013, Zhang et al. [34] studied a series of SB FH compounds and found that some SB compounds with the XA structure can exhibit nontrivial topological band ordering. In 2017, Li et al. [35] studied the thermoelectric characteristics of FH Sc_2FeSi and Sc_2FeGe and found maximum power factors of 48.77×10^{14} μW cm^{-1} K^{-2} s^{-1} and 47.11×10^{14} μW cm^{-1} K^{-2} s^{-1} for Sc_2FeSi and Sc_2FeGe, respectively.

In this study, we will focus on a new FH alloy, Sc_2VGe, and perform a complete first-principle study of the site-preference, electronic, magnetic, and half-metallic properties of this material. Further, phase stability in terms of the calculated formation and cohesive energies is also explained. Moreover, the conduction band minimum (CBM), valence band maximum (VBM), band gap and half-metallic band gap, total and atomic magnetic moments, and electronic band structures as functions of the lattice parameter and c/a ratio will be discussed in detail.

2. Calculation Methods

In this study, the plane-wave pseudopotential method within CASTEP [36], which uses density functional theory, was used to calculate the physical properties of the material. The generalized gradient approximation (GGA) [37] was used in the scheme of Perdew–Burke–Ernzerh of (PBE) [38] to deal with the exchange and correlation functions between electrons. The cutoff energy for plane waves was set to 450 eV, and the convergence was set to 5×10^{-7} eV using $12 \times 12 \times 12$ mesh points grid. The above parameters ensure the accuracy of the calculated results based on the references [39]. Similar methods to investigate the electronic structures of Heusler alloys can be found in [30–33].

3. Results and Discussions

3.1. Competition of $L2_1$ and XA Structurein Full-Heusler Sc_2VGe

It is well known that there are four atomic sites for FH alloys, i.e., A (0, 0, 0), B (0.25, 0.25, 0.25), C (0.5, 0.5, 0.5), and D (0.75, 0.75, 0.75). When atomic occupancy is X (A)-X (B)-Y (C)-Z (D), the XA structure is formed; on the other hand, when atomic occupancy is X (A)-Y (B)-X (C)-Z (D), the $L2_1$ structure is formed [40]. For Sc_2VGe compound, the two structures are shown in Figure 1. According to the traditional SPR [40–45], the V atom has more valence electrons than the Sc atom and tends to occupy the C position, the two Sc atoms occupy A and B positions, respectively, and the Ge atom occupies the D position, thus, preferring to form the XA structure. However, we should point out that traditional SPR may not be suitable for all FH alloys. Therefore, for both the types, we focused on the relationship between their total energies during FM state and lattice parameters in this study. From Figure 2 and Table 1, we see that $L2_1$ type has a lower total energy; therefore, $L2_1$-type structure is considered more stable than the XA type. Interestingly, the calculated results are contrary to that of SPR, that is, here, the most stable structure of Heusler Sc_2VGe alloy is found to be the $L2_1$ type instead of XA type. For the XA-type Sc_2VGe, the calculated magnetic moment is 3 μ_B and it conforms well to the Slater–Pauling rule: $M_t = Z_t - 18$ [46,47].

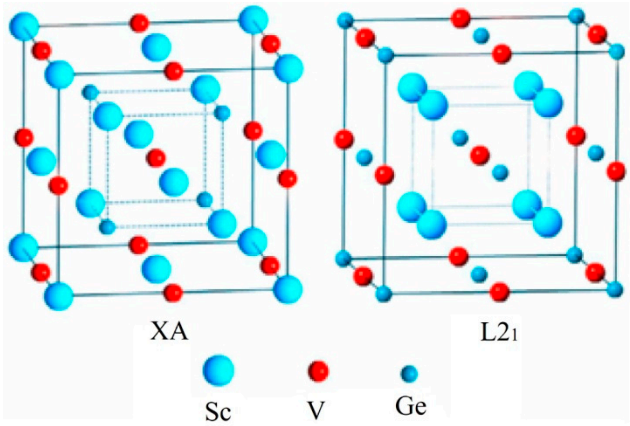

Figure 1. Crystal structures of XA and $L2_1$-type for Sc_2VGe compound.

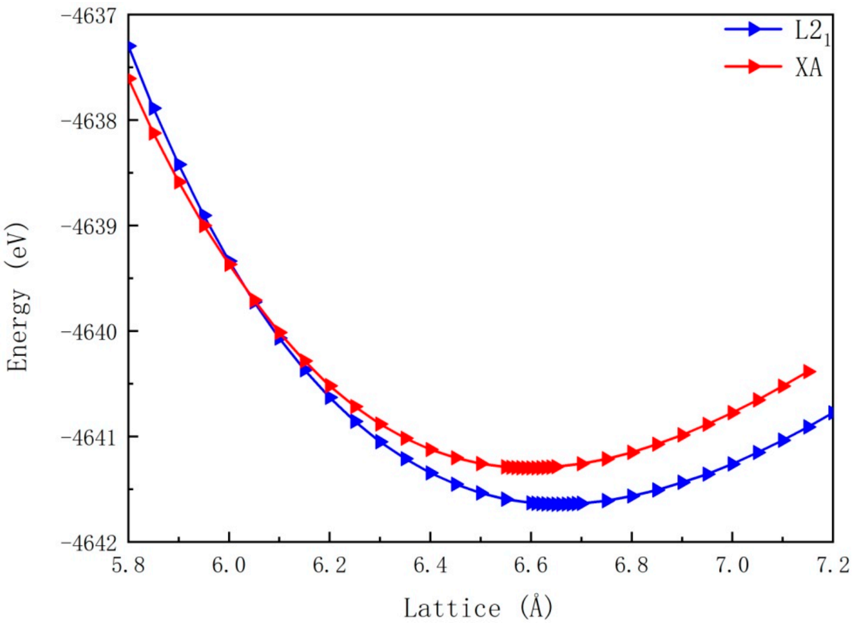

Figure 2. Between the lattice parameter and the total energy for Sc_2VGe compound with XA and $L2_1$ structures. The energies in this figure were calculated per unit cell of Sc_2VGe.

Table 1. Calculated total and atomic magnetic moments and total energy for Sc_2VGe compound. The energies in this table were calculated per unit cell of Sc_2VGe.

Type	M_{total} (μ_B)	M_{Sc} (μ_B)	M_{Sc} (μ_B)	M_V (μ_B)	M_{Ge} (μ_B)	Energy (eV)
XA	3.00	−0.28	0.53	3.07	−0.32	−4641.30
$L2_1$	2.93	−0.01	−0.01	3.22	−0.27	−4641.64

We further calculated the band structures of the two types of Sc_2VGe compound. It can be noted from Figure 3 that XA-type Sc_2VGe (Figure 3a) is a HM with a direct band gap (at point G). Furthermore, the spin-up channel of Sc_2VGe exhibits semiconducting property and the spin-down channel of it shows a metallic behavior. Based on the obtained band structures of XA-type Sc_2VGe, we can see that 100% spin polarization [48,49] occurs near the Fermi level. On the other hand, $L2_1$-type Sc_2VGe (Figure 3b) shows metallic behavior. In short, the band structures for both the spin channels in the Fermi level overlap with each other and reflect a metallic behavior.

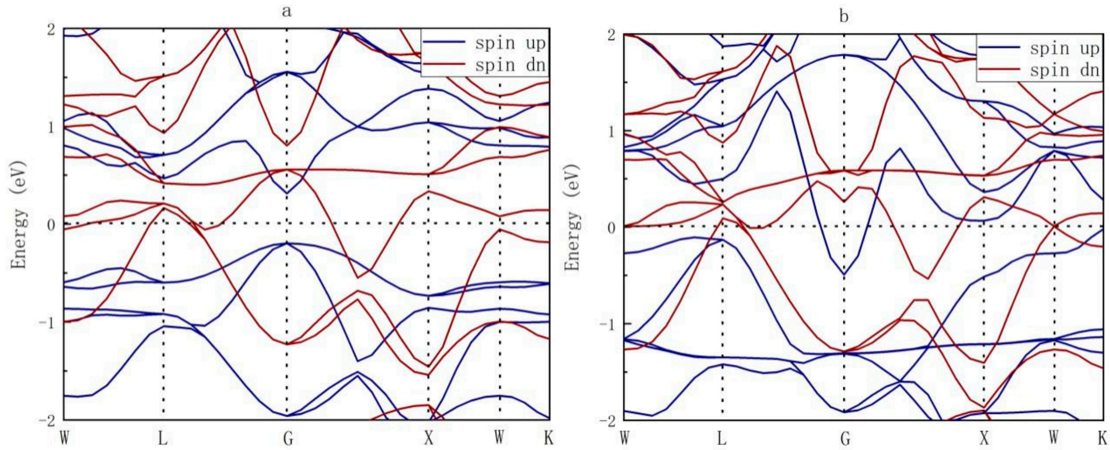

Figure 3. Band structures for Sc_2VGe: (**a**) XA type and (**b**) $L2_1$ type.

3.2. Thermal Stability of XA-Type Sc_2VGe

To determine the stability of XA-type Sc_2VGe compound, the cohesive energy (E_c) was calculated. The E_c per unit cell can be expressed using the following formula [50]:

$$E_C = 2E_{Sc}^{iso} + E_V^{iso} + E_{Ge}^{iso} - E_{total}^{Sc_2VGe} \quad (1)$$

where $E_{total}^{Sc_2VGe}$ is the total energy of the Sc_2VGe compound, E_{Sc}^{iso}, E_V^{iso}, and E_{Ge}^{iso} are the energies of the isolated atoms Sc, V, and Ge, respectively. The calculated E_c of Sc_2VGe compound is 20.62 eV, indicating that the chemical bonding of Sc_2VGe compound is firm.

In addition, formation energy (E_f) is another way to describe the stability of crystals. We use the following formula to characterize E_f per unit cell of Sc_2VGe [50]:

$$E_f = E_{total}^{Sc_2VGe} - 2E_{bulk}^{Sc} - E_{bulk}^{V} - E_{bulk}^{Ge} \quad (2)$$

where $E_{total}^{Sc_2VGe}$ is the same as mentioned above, E_{bulk}^{Sc}, E_{bulk}^{V}, and E_{bulk}^{Ge} are energies of Sc, V, and Ge bulks, respectively. The calculated E_f of Sc_2VGe compound is −3.64 eV, which is a negative value theoretically indicating that Sc_2VGe compound is thermally stable.

Based on the results of E_c and E_f, it can be said that the XA-type Sc_2VGe compound is found to be stable in terms of theory. We hope this material can be experimentally synthesized in the near future.

3.3. Total and Partial Density of States of XA-Type Sc_2VGe

To analyze the contribution of each atom to the energy bands, we calculated the total density of states (TDOS) and the partial density of states (PDOS) for each atom. It can be seen from Figure 4 that the low range of energy states (lower than −2 eV) of TDOS are mainly due to the contribution of the atoms of the main group element Ge, such as the peak in the energies between −4 eV and −5 eV and peak in the energies between −3 eV and −2 eV. There are two obvious peaks in spin-up channels near the Fermi level that range from −1 eV to 0 eV, and the main TDOS in this range comes from the contributions of V atom. Further, Sc_1 and Sc_2 atoms also contribute a small part to the energy states from −1 eV to 0 eV. Near the Fermi level, the TDOS of the spin-up channel is zero and has a large energy gap, whereas the spin-down channel is not zero, which mainly results from the hybridization among Sc_1, Sc_2, and V atoms. From the DOS, similar to the calculated band structures, one can see that half-metallic property with full spin polarization is found in XA-type Sc_2VGe. Moreover, from the TDOS, we can see that the energy gap in the spin-up direction is generated by four peaks, two peaks below, and two peaks above the Fermi level. As discussed previously, the two peaks below the Fermi level are mainly derived from the d orbital of V atoms. The two peaks above the Fermi level, as can be clearly seen, are mainly derived from the *d* orbital of Sc atoms. Moreover, the hybridization of *d*-*d* orbitals between V and Sc atoms plays an important role, which cannot be ignored, in the formation of energy gap in the spin-up channel.

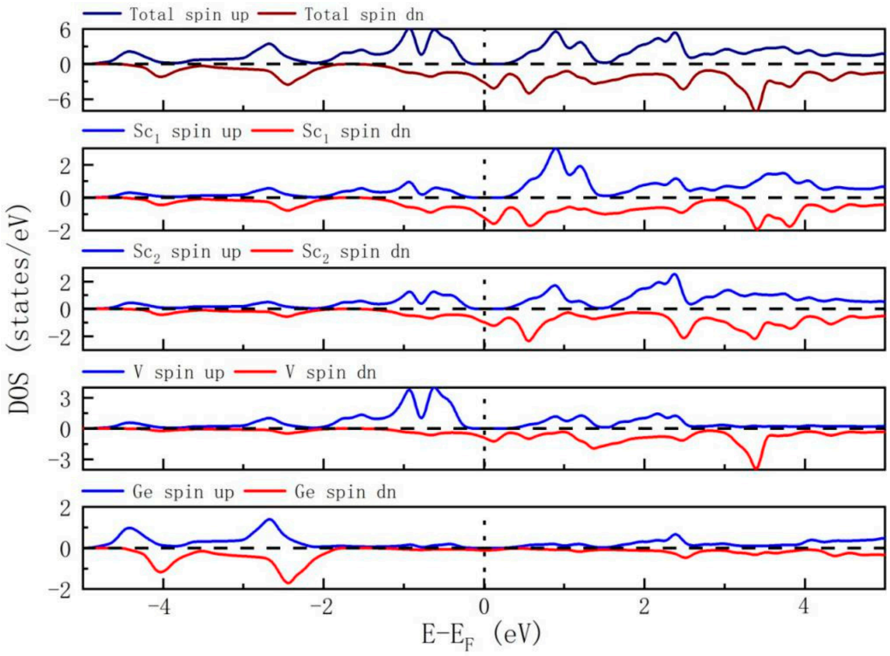

Figure 4. Density of states (TDOS) and partial density of states (PDOS) for XA-type Sc_2VGe.

3.4. Effect of Uniform Strain on XA-Type Sc_2VGe

Uniform strain is an important way to regulate the band structures, i.e., the physics nature of alloys. In this section, we will discuss the effect of uniform strain on the band structures of XA-type Sc_2VGe alloy. Firstly, we aim to study the physical nature transition of XA-type Sc_2VGe as the lattice parameter changes from 5.80 Å to 7.20 Å. The results are shown in Figure 5. When the lattice parameter of XA-type Sc_2VGe is smaller than 6.16 Å, it is considered to be a magnetic metal, as shown in Figure 5a. When the lattice parameter is between 6.16 Å and 6.54 Å (see Figure 5b), XA-type Sc_2VGe is a HM material with an indirect band gap in the spin-up channel. When the lattice parameter is between 6.54 Å and 6.69 Å, half-metallic behavior with direct band gap can be found in the XA-type Sc_2VGe, as exhibited in Figure 5c,d. When the lattice parameter is larger than 6.69 Å, the HM property of this alloy breaks and a metallic property appears instead.

Figure 6a shows the calculated CBM, VBM, band gap, and half-metallic band gap in the spin-up channel at different lattice parameters for XA-type Sc_2VGe. One can see that the half-metallic band gap gradually increases from 6.2 Å, and then gradually decreases after reaching a maximum value at 6.6 Å, and finally disappears at approximately 6.7 Å. More importantly, the maximum half-metallic band gap at around 6.6 Å is about 0.2 eV. Such a large value ensures that the half-metallic property of this material is not affected by external factors. On the other hand, we can see that the band gap in the spin-up direction of this material almost remains constant over the lattice range of 6.2 Å to 6.4 Å. When the lattice parameter is in the range of 6.4 Å to 6.7 Å, the band gap is significantly reduced.

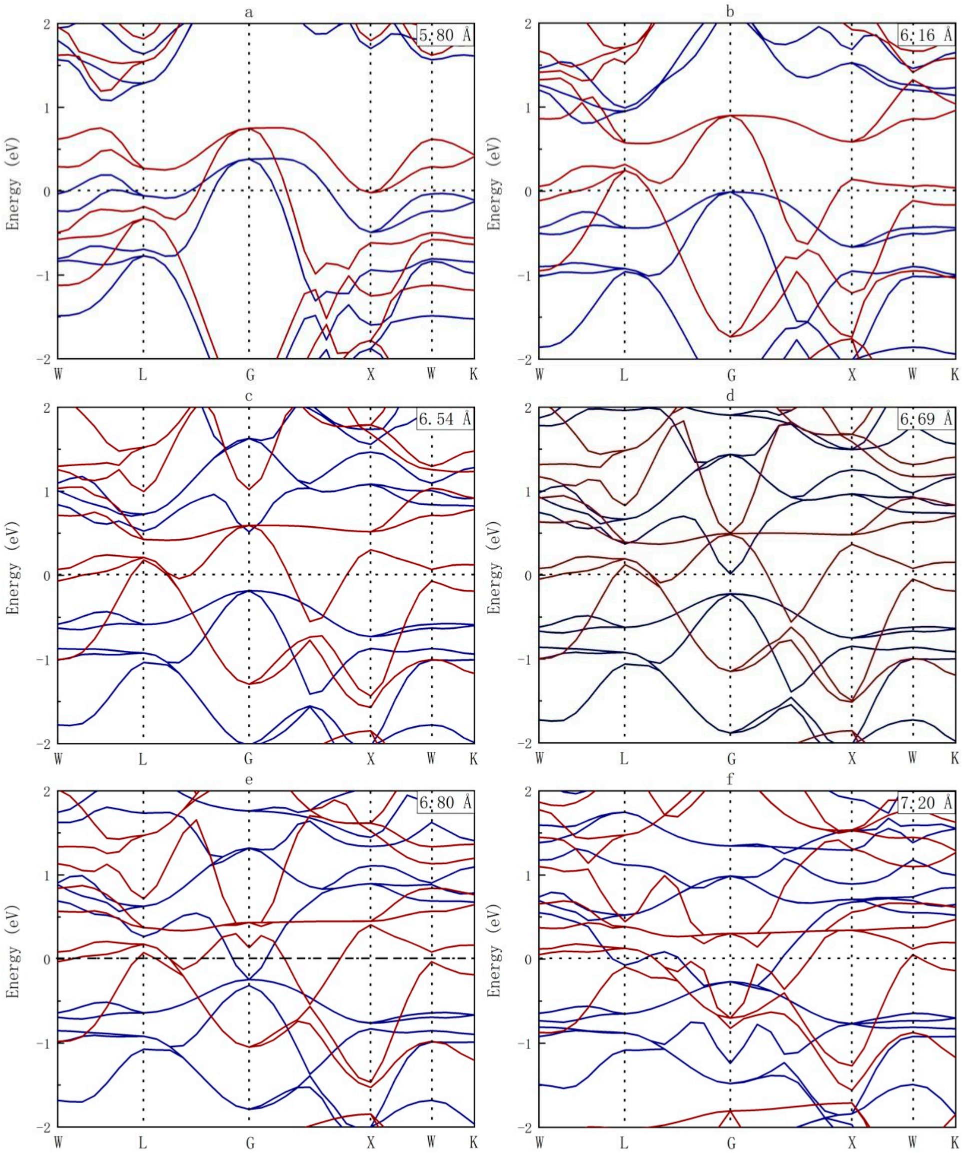

Figure 5. Band structures for the XA-type Sc_2VGe at its uniform strained lattice parameters. The blue lines represent the spin-up channel.

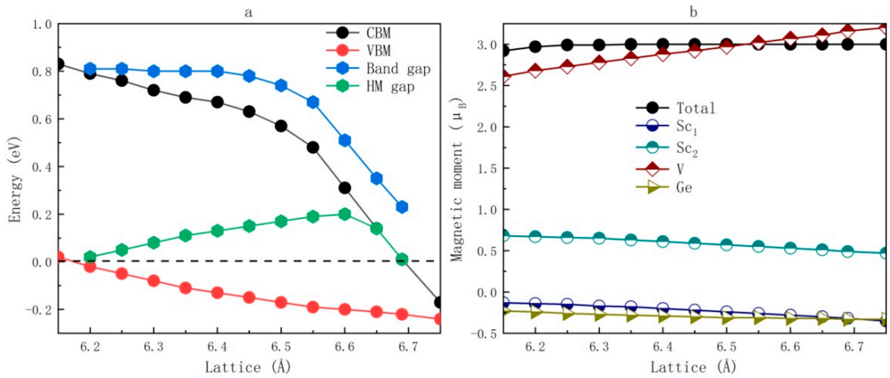

Figure 6. (**a**) band minimum (CBM), valence band maximum (VBM), Band gaps, and half-metal (HM) gaps of the spin-up channel bands as a function of lattice parameter, and (**b**) the total and atomic magnetic moments as a function of lattice parameter for XA-type Sc_2VGe.

The total and atomic magnetic moments under uniform strain were also studied. The results are shown in Figure 6b. We can see that the total magnetic moment of XA-type Sc_2VGe hardly changes as the lattice parameter changes. For atomic magnetic moments, as the lattice parameters increase, the atomic magnetic moment of V gradually increases, while the atomic magnetic moments of other atoms gradually decrease.

3.5. The effect of Tetragonal Lattice Distortion on XA-Type Sc_2VGe

The effect of tetragonal distortion on the electronic structures of XA-type Sc_2VGe was studied. Firstly, we studied the physical transition during a change in the c/a ratio when in the range of 0.75~1.25. As shown in Figure 7, when the range of c/a ratio is between 0.80 to 1.22 (see Figure 7b–e), the compound shows the HM property. On the other hand, it is a metal when the c/a ratio is lower than 0.80 (see Figure 7a) or higher than 1.22 (see Figure 7f).

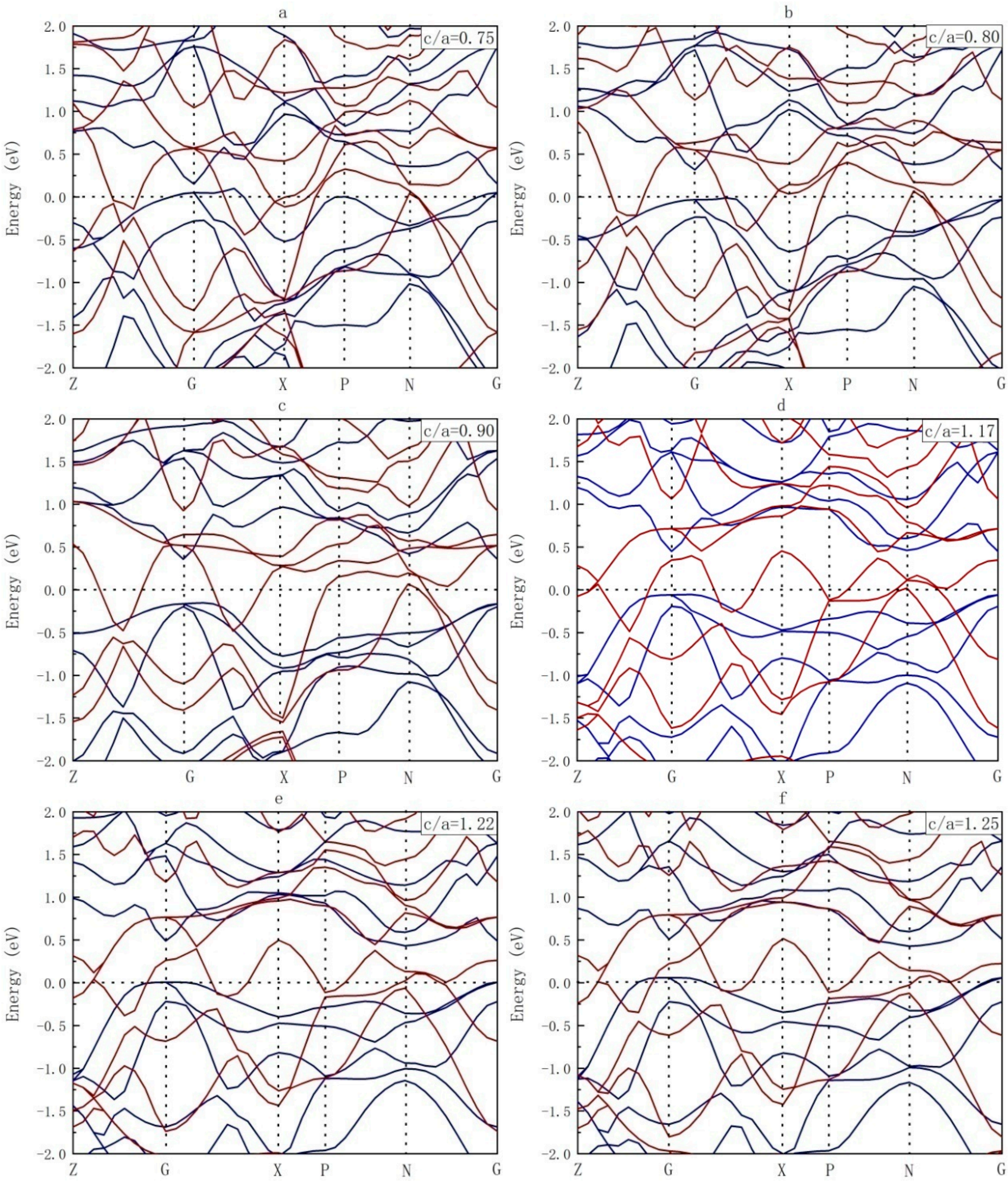

Figure 7. Band structures for the XA-type Sc_2VGe at its tetragonal distortion lattice parameters.

As shown in Figure 8a, the largest HM gap appears when c/a=1. As the c/a ratio increases (or decreases), the VBM in the spin-up channel gradually decreases, and therefore, the HM band gap decreases. The band gap does not change much when the c/a ratio is in the range of 0.85 to 1.15. The reason behind this can be understood from Figure 8a. In this interval, when c/a increases or decreases, although the VBM always decreases, the CBM shows an increasing trend, such that the overall band gap remains almost unchanged.

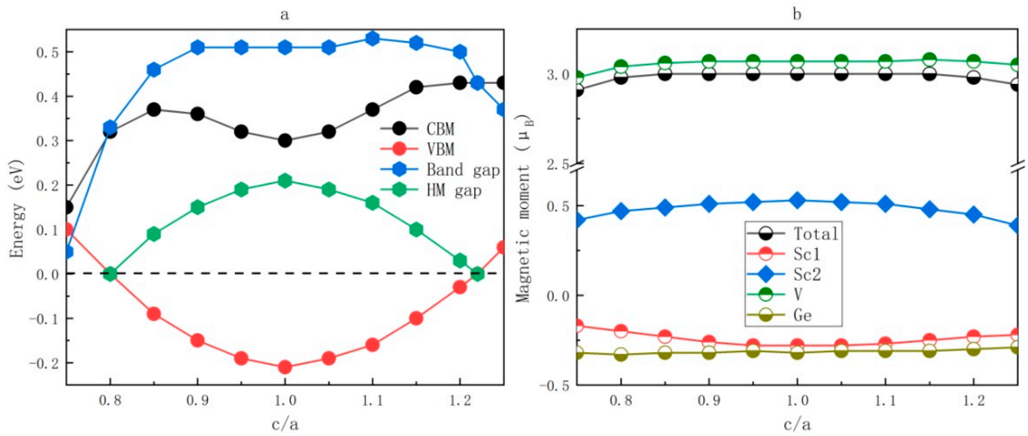

Figure 8. (**a**) VBM, Bandgaps, and HM gaps of the spin-up channel band as a function of c/a for XA-type Sc_2VGe, and (**b**) the total and atomic magnetic moments as a function of c/a for XA-type Sc_2VGe.

Finally, we study the effect of tetragonal distortion of XA-type Sc_2VGe on its magnetic property. It can be seen from Figure 8b that the magnetic moments of unit cell and each atom vary slightly when the c/a ratio ranges from 0.75 to 1.25, which show that the magnetism of the material is quite stable and has a strong resistance to tetragonal lattice distortion.

4. Conclusions

In this study, we focused on FH alloy Sc_2VGe, and showed a complete first-principle study on the site-preference, electronic, magnetic, and half-metallic properties of this material. The main results are as follows:

(i) The site-preference of FH alloy Sc_2VGe was examined, and results showed that the $L2_1$ type is more stable than the XA type. We further calculated the electronic structures of both types of Sc_2VGe and found that the XA-type alloy was an excellent half-metallic material, whereas the $L2_1$-type alloy was a magnetic metal. XA-type Sc_2VGe can intrinsically provide single spin channel electrons, and therefore this material can be used for pure spin generation and injection.

(ii) When XA-type Sc_2VGe is at its equilibrium lattice parameter, its total magnetic moment is 3 μ_B, which is in accordance with the well-known Slater–Pauling rule, and the main contribution to the total magnetism came from V atoms.

(iii) The effects of uniform strain and tetragonal lattice distortion on the electronic structures of XA-type Sc_2VGe were also studied. We found that the half-metallic state can be maintained in a large area of the lattice parameter and the c/a ratio, indicating that XA-type Sc_2VGe is a robust half-metallic material.

(iv) The formation energy and cohesive energy were calculated and results showed that this alloy has extensive scope for use in experiments.

(v) The half-metallic band gap and the band gap in the spin-up channel as a function of the lattice parameter and the c/a ratio were taken into consideration for XA-type Sc_2VGe, and we found that the maximum half-metallic band gap around 6.6 Å was approximately 0.2 eV. Such a large value ensures that the half-metallic property of this material is not affected by external factors.

(vi) All the aforementioned results indicate that XA-type Sc_2VGe would be an ideal candidate in spintronics.

Author Contributions: Methodology, Z.C.; software, Z.C.; investigation, Z.C., H.X.; writing—original draft preparation, Z.C.; writing—review and editing, Y.G.; supervision, X.W., T.Y., Y.G.

Funding: This research received no external funding.

Conflicts of Interest: The authors declare no conflict of interest.

References

1. Groot, R.A.D.; Mueller, F.M.; Engen, P.G.V.; Buschow, K.H.J. New class of materials: Half-metallic ferromagnets. *Phys. Rev. Lett.* **1983**, *50*, 2024–2027. [CrossRef]
2. Haque, E.; Hossain, M.A. First-principles study of elastic, electronic, thermodynamic, and thermoelectric transport properties of TaCoSn. *Results Phys.* **2018**, *10*, 458–465. [CrossRef]
3. Tang, Y.; Li, X.; Martin, H.J.; Reyes, E.C.; Ivas, T.; Leinenbach, C.; Anand, S.; Peters, M.; Snyde, G.; Battaglia, C. Impact of Ni content on the thermoelectric properties of half-Heusler TiNiSn. *Energy Environ. Sci.* **2018**, *11*, 311–320. [CrossRef]
4. Liu, Y.; Fu, C.; Xia, K.; Yu, J.; Zhao, X.; Pan, H.; Felser, C.; Zhu, T.J. Lanthanide Contraction as a Design Factor for High-Performance Half-Heusler Thermoelectric Materials. *Adv. Mater.* **2018**, *30*, 1800881. [CrossRef] [PubMed]
5. Zhang, Y.J.; Liu, Z.H.; Wu, Z.G.; Ma, X.Q. Prediction of fully compensated ferrimagnetic spin-gapless semiconducting FeMnGa/Al/In half Heusler alloys. *IUCrJ* **2019**, *6*, 610–618. [CrossRef] [PubMed]
6. Han, Y.; Bouhemadou, A.; Khenata, R.; Cheng, Z.; Yang, T.; Wang, X. Prediction of possible martensitic transformations in all-*d*-metal Zinc-based Heusler alloys from first-principles. *J. Magn. Magn. Mater.* **2019**, *471*, 49–55. [CrossRef]
7. Anjami, A.; Boochani, A.; Elahi, S.M.; Akbari, H. Ab-initio study of mechanical, half-metallic and optical properties of Mn_2ZrX (X= Ge, Si) compounds. *Results Phys.* **2017**, *7*, 3522–3529. [CrossRef]
8. Faleev, S.V.; Ferrante, Y.; Jeong, J.; Samant, M.G.; Jones, B.; Stuart, P. Origin of the tetragonal ground state of Heusler compounds. *Phys. Rev. Appl.* **2017**, *7*, 034022. [CrossRef]
9. Sanvito, S.; Oses, C.; Xue, J.; Tiwari, A.; Zic, M.; Archer, T.; Tozman, P.; Venkatesan, M.; Coey, M.; Curtarolo, S. Accelerated discovery of new magnets in the Heusler alloy family. *Sci. Adv.* **2017**, *3*, e1602241. [CrossRef] [PubMed]
10. Xin, Y.; Ma, Y.; Hao, H.; Luo, H.; Meng, F.; Liu, H.; Liu, E.; Wu, G. Structure and magnetic properties of Heusler alloy Co_2RuSi melt-spun ribbons. *J. Magn. Magn. Mater.* **2017**, *435*, 76–80. [CrossRef]
11. Li, T.; Wu, Y.; Han, Y.; Wang, X. Tuning the topological nontrivial nature in a family of alkali-metal-based inverse Heusler compounds: A first-principles study. *J. Magn. Magn. Mater.* **2018**, *463*, 44–49. [CrossRef]
12. Galdun, L.; Ryba, T.; Prida, V.M.; Zhukova, V.; Zhukov, A.; Diko, P.; Kavečanský, V.; Vargova, Z.; Varga, R. Monocrystalline Heusler Co_2FeSi alloy glass-coated microwires: Fabrication and magneto-structural characterization. *J. Magn. Magn. Mater.* **2018**, *453*, 96–100. [CrossRef]
13. Marchenkov, V.V.; Perevozchikova, Y.A.; Kourov, N.I.; Irkhin, V.Y.; Eisterer, M.; Gao, T. Peculiarities of the electronic transport in half-metallic Co-based Heusler alloys. *J. Magn. Magn. Mater.* **2018**, *459*, 211–214. [CrossRef]
14. Hu, Y.; Zhang, J.M. First-principles study of the Hf-based Heusler alloys: Hf_2CoGa and Hf_2CoIn. *J. Magn. Magn. Mater.* **2017**, *421*, 1–6. [CrossRef]
15. Ahmad, N.; Ahmed, N.; Han, X.F. Analysis of electronic, magnetic and half-metallic properties of $L2_1$-type ($Co_2Mn_{0.5}Fe_{0.5}Sn$) Heusler alloy nanowires synthesized by AC-electrodeposition in AAO templates. *J. Magn. Magn. Mater.* **2018**, *460*, 120–127.
16. Djefal, A.; Amari, S.; Obodo, K.O.; Beldi, L.; Bendaoud, H.; Evans, R.F.L.; Bouhafs, B. Half-metallic ferromagnetism in double perovskite Ca_2CoMoO_6 compound: DFT + U calculations. *Spin* **2017**, *7*, 1750009. [CrossRef]
17. Yan, W.; Zhang, X.; Shi, Q.; Yu, X.; Zhang, Z.; Wang, Q. Study of magnetocaloric effect in half-metallic ferromagnet $Co_3Sn_2S_2$. *Results Phys.* **2018**, *11*, 1004–1007.

18. Li, Y.; Liu, G.D.; Wang, X.T.; Liu, E.K.; Xi, X.K.; Wang, W.H.; Wu, G.H.; Wang, L.Y.; Dai, X.F. First-principles study on electronic structure, magnetism and half-metallicity of the NbCoCrAl and NbRhCrAl compounds. *Results Phys.* **2017**, *7*, 2248–2254. [CrossRef]
19. Akbar, W.; Nazir, S. Origin of p-type half-metallic ferromagnetism in carbon-doped BeS: First-principles characterization. *J. Alloy. Compd.* **2018**, *743*, 83–86. [CrossRef]
20. Yousuf, S.; Gupta, D.C. Insight into half-metallicity, spin-polarization and mechanical properties of $L2_1$ structured MnY_2Z (Z = Al, Si, Ga, Ge, Sn, Sb) Heusler alloys. *J. Alloy. Compd.* **2018**, *735*, 1245–1252. [CrossRef]
21. Boehnke, A.; Martens, U.; Sterwerf, C.; Niesen, A.; Huebner, T.; Ehe, M.; Meinert, M.; Kuschel, T.; Thomas, A.; Heiliger, C.; et al. Large magneto-Seebeck effect in magnetic tunnel junctions with half-metallic Heusler electrodes. *Nat. Commun.* **2017**, *8*, 1626. [CrossRef]
22. Zhang, L.; Wang, X.; Cheng, Z. Electronic, magnetic, mechanical, half-metallic and highly dispersive zero-gap half-metallic properties of rare-earth-element-based quaternary Heusler compounds. *J. Alloy. Compd.* **2017**, *718*, 63–74. [CrossRef]
23. Chadov, S.; Wu, S.C.; Felser, C.; Galanakis, I. Stability of Weyl points in magnetic half-metallic Heusler compounds. *Phys. Rev. B* **2017**, *96*, 024435. [CrossRef]
24. Chen, J.; Gao, G.Y.; Yao, K.L.; Song, M.H. Half-metallic ferromagnetism in the half-Heusler compounds GeKCa and SnKCa from first-principles calculations. *J. Alloy. Compd.* **2011**, *509*, 10172–10178. [CrossRef]
25. Yao, Z.; Zhang, Y.S.; Yao, K.L. Large half-metallic gap in ferromagnetic semi-Heusler alloys CoCrP and CoCrAs. *Appl. Phys. Lett.* **2012**, *101*, 062402. [CrossRef]
26. Hirohata, A.; Sagar, J.; Lari, L.; Fleet, L.R.; Lazarov, V.K. Heusler-alloy films for spintronic devices. *Appl. Phys. A* **2013**, *111*, 423–430. [CrossRef]
27. Azadani, J.; Munira, K.; Romero, J.; Ma, J.; Sivakumar, C.; Ghosh, A.W.; Butler, W.H. Anisotropy in layered half-metallic Heusler alloy superlattices. *J. Appl. Phys.* **2016**, *119*, 043904. [CrossRef]
28. Nazemi, N.; Ahmadian, F. Half-Metallic Characteristic in the New Full–Heusler $SrYO_2$ (Y = Sc, Ti, V, and Cr). *Phys. Solid State* **2019**, *61*, 1–10. [CrossRef]
29. Kogachi, M.; Fujiwara, T.; Kikuchi, S. Atomic disorder and magnetic property in Co-based heusler alloys Co_2MnZ (Z = Si, Ge, Sn). *J. Alloy. Compd.* **2009**, *475*, 723–729. [CrossRef]
30. Liu, G.D.; Dai, X.F.; Liu, H.Y.; Chen, J.L.; Li, Y.X.; Xiao, G.; Wu, G.H. Mn_2CoZ (Z = Al, Ga, In, Si, Ge, Sn, Sb) compounds: Structural, electronic, and magnetic properties. *Phys. Rev. B* **2008**, *77*, 117–119. [CrossRef]
31. Wang, X.T.; Cui, Y.T.; Liu, X.F.; Liu, G.D. Electronic structures and magnetism in the Li_2AgSb-type heusler alloys, Zr_2CoZ (Z = Al, Ga, In, Si, Ge, Sn, Sb, Pb, Sb): A first-principles study. *J. Magn. Magn. Mater.* **2015**, *394*, 50–59. [CrossRef]
32. Wang, X.T.; Cheng, Z.X.; Yuan, H.K.; Khenata, R. $L2_1$ and XA ordering competition in Titanium-based full-heusler alloys. *J. Mater. Chem. C* **2017**, *5*, 11559–11564. [CrossRef]
33. Wang, X.T.; Cheng, Z.X.; Wang, W.H. $L2_1$ and XA ordering competition in hafnium-based full-heusler alloys Hf_2VZ (Z = Al, Ga, In, Tl, Si, Ge, Sn, Pb). *Materials* **2017**, *10*, 1200. [CrossRef]
34. Zhang, X.M.; Liu, E.K.; Liu, Z.Y.; Liu, G.D.; Wu, G.H.; Wang, W.H. Prediction of topological insulating behavior in inverse Heusler compounds from first principles. *Comput. Mater. Sci.* **2013**, *70*, 145–149. [CrossRef]
35. Li, J.; Yang, G.; Yang, Y.; Ma, H.; Zhang, Q.; Zhang, Z.; Fang, W.; Yin, F.; Li, J. Electronic and thermoelectric properties of nonmagnetic inverse Heusler semiconductors Sc_2FeSi and Sc_2FeGe. *J. Magn. Magn. Mater.* **2017**, *442*, 151–158. [CrossRef]
36. Segall, M.D.; Lindan, P.J.; Probert, M.A.; Pickard, C.J.; Hasnip, P.J.; Clark, S.J.; Payne, M.C. First-principles simulation: Ideas, illustrations and the CASTEP code. *J. Phys.* **2002**, *14*, 2717. [CrossRef]
37. Perdew, J.P.; Burke, K.; Ernzerhof, M. Generalized gradient approximation made simple. *Phys. Rev. Lett.* **1996**, *77*, 3865–3868. [CrossRef]
38. Maximoff, S.N.; Ernzerhof, M.; Scuseria, G.E. Current-dependent extension of the Perdew-Burke-Ernzerhof exchange-correlation functional. *J. Chem. Phys.* **2004**, *120*, 2105–2109. [CrossRef]
39. Chen, Z.; Rozale, H.; Gao, Y.; Xu, H. Strain Control of the Tunable Physical Nature of a Newly Designed Quaternary Spintronic Heusler Compound ScFeRhP. *Appl. Sci.* **2018**, *8*, 1581. [CrossRef]
40. Galanakis, I.; Dederichs, P.H.; Papanikolaou, N. Slater-Pauling behavior and origin of the half-metallicity of the full-Heusler alloys. *Phys. Rev. B* **2002**, *66*, 174429. [CrossRef]

41. Skaftouros, S.; Özdoğan, K.; Şaşıoğlu, E.; Galanakis, I. Generalized Slater-Pauling rule for the inverse Heusler compounds. *Phys. Rev. B* **2013**, *87*, 024420. [CrossRef]
42. Meng, F.; Hao, H.; Ma, Y.; Guo, X.; Luo, H. Site preference of Zr in Heusler alloys Zr_2YAl (Y = Cr, Mn, Fe, Co, Ni) and its influence on the electronic properties. *J. Alloy. Compd.* **2017**, *695*, 2995–3001. [CrossRef]
43. Ni, Z.; Ma, Y.; Liu, X.; Luo, H.; Liu, H.; Meng, F. Site preference, electronic structure and possible martensitic transformation in Heusler alloys Ni_2CoZ (Z = Al, Ga, In, Si, Ge, Sn, Sb). *Intermetallics* **2017**, *81*, 1–8.
44. Ma, Y.; Hao, H.; Xin, Y.; Luo, H.; Liu, H.; Meng, F.; Liu, E. Atomic ordering and magnetic properties of quaternary Heusler alloys NiCuMnZ (Z = In, Sn, Sb). *Intermetallics* **2017**, *86*, 121–125. [CrossRef]
45. Luo, H.; Xin, Y.; Liu, B.; Men, F.; Li, H.; Liu, E.; Wu, G. Competition of $L2_1$ and XA structural ordering in Heusler alloys X_2CuAl (X = Sc, Ti, V, Cr, Mn, Fe, Co, Ni). *J. Alloy. Compd.* **2016**, *665*, 180–185. [CrossRef]
46. Wang, J.X.; Chen, Z.B.; Gao, Y.C. Phase stability, magnetic, electronic, half-metallic and mechanical properties of a new equiatomic quaternary Heusler compound ZrRhTiIn: A first-principles investigation. *J. Phys. Chem. Solids* **2018**, *116*, 72–78. [CrossRef]
47. Han, Y.; Wu, Y.; Li, T.; Khenata, R.; Yang, T.; Wang, X. Electronic, magnetic, half-metallic, and mechanical properties of a new equiatomic quaternary Heusler compound YRhTiGe: A first-principles study. *Materials* **2018**, *11*, 797. [CrossRef] [PubMed]
48. Chandra, A.R.; Jain, V.; Lakshmi, N.; Jain, V.K.; Jain, R.; Venugopalan, K. Spin polarization in Co_2CrAl/GaAs 2D-slabs: A computational study. *J. Magn. Magn. Mater.* **2018**, *448*, 75–81. [CrossRef]
49. Bhat, T.M.; Gupta, D.C. First-principles study of high spin-polarization and thermoelectric efficiency of ferromagnetic CoFeCrAs quaternary Heusler alloy. *J. Magn. Magn. Mater.* **2018**, *449*, 493–499. [CrossRef]
50. Wang, X.; Cheng, Z.; Liu, G.; Dai, X.; Bouhemadou, A. Rare earth-based quaternary Heusler compounds MCoVZ (M = Lu, Y.; Z= Si, Ge) with tunable band characteristics for potential spintronic applications. *IUCrJ* **2017**, *4*, 758–768. [CrossRef] [PubMed]